Bilayers in nanoparticle-doped polar mesogens

Alexander Lorenz,[1] Deña M. Agra-Kooijman,[2] Natalie Zimmermann,[3] Heinz-S. Kitzerow,[3]
Dean R. Evans,[4] and Satyendra Kumar[2]

[1]*Department of Engineering, University of Cambridge, 9 JJ Thompson Avenue, CB3 0FA Cambridge, United Kingdom*
[2]*Department of Physics, Kent State University, Kent, Ohio 44242, USA*
[3]*Department of Chemistry, University of Paderborn, Warburger Strasse 100, 33098 Paderborn, Germany*
[4]*Air Force Research Laboratory, Materials and Manufacturing Directorate, Wright-Patterson Air Force Base, Ohio 45433, USA*

(Received 19 September 2013; published 10 December 2013)

Structures of the mesophases of five members of the 4-*n*-alkyl-4′-cyanobiphenyl homologous series (4-*n*-butyl-4′-cyanobiphenyl to 4-*n*-octyl-4′-cyanobiphenyl) doped with milled $BaTiO_3$ nanoparticles were investigated by x-ray scattering. Clear solutions of each of the 4-*n*-alkyl-4′-cyanobiphenyls were first prepared in *n*-heptane and then doped with an *n*-heptane/nanoparticle dispersion, which led to gelation. The nanogels were found to be one-dimensional, multilayered, smectic nanostructures in each case. Surprisingly, a characteristic layer spacing of 4.5 nm was observed in all five homologues. Synchrotron x-ray scattering study of the multilayer structures of doped 4-*n*-pentyl-4′-cyanobiphenyl and 4-*n*-octyl-4′-cyanobiphenyl revealed nine orders of the primary Bragg reflection which were used to calculate the electron density profiles of the multilayers by Fourier analysis. The multilayers were found to consist of molecular bilayers wherein the mesogens were arranged in a head-to-head assembly of the polar head groups. The alkyl tails of the mesogenic molecules were freely movable and the tail-to-tail assembly was stabilized by heptane. The dissolved nanoparticles clearly induced a new self-assembled nanostructure in which the rigid aromatic part, and not the overall length, of the molecules defined the layer spacing.

DOI: 10.1103/PhysRevE.88.062505 PACS number(s): 61.30.Eb, 61.05.cf, 64.75.Jk

I. INTRODUCTION

Beneficial modifications of the structure and properties of functional soft organic materials such as liquid crystals (LCs) can be achieved by doping them with a small amount of inorganic nanoparticles. The effect of various types of nanoparticles on LCs has been investigated. The impact of solid nanoparticles on phases of soft materials depends greatly on the material and on the surface functionalization of nanoparticles [1,2]. New phenomena and material properties are observed if the surface functionalization consists of covalently bonded protomesogenic ligands. Such nanoparticles can self-assemble into nanoparticulate thermotropic liquid crystalline materials [3,4]. In contrast, silica nanoparticles with covalently bonded alkyl-type surface functionalization [5] can improve the electro-optical performance of LCs or lead to dual alignment effects [6]. Silica nanoparticles free of surface functionalization are suitable to fabricate bistable display devices with the capability of selective erasure using optical fields [7,8]. Additionally, they create memory effects that are addressable by quasistatic electric or magnetic fields [9]. It was deduced that such permanent memory is very likely caused by a surface memory effect well known for planar substrates, where a surface-induced thin adsorbed layer of a lower-temperature crystalline phase of the mesogen is present at the solid-LC interface [10].

Surfactants, such as oleic acid, have been used for non-covalently bonded surface functionalization to obtain stable nanodispersions of inorganic nanoparticles in organic solvents. It is possible to prepare dispersions of $BaTiO_3$ nanoparticles by milling cubic $BaTiO_3$ in heptane in the presence of a small amount of oleic acid in a planetary ball mill [11,12]. From these dispersions, stressed $BaTiO_3$ nanoparticles, which possess permanent electric polarization, can be harvested [13]. Generally, doping of LCs with milled $BaTiO_3$ nanoparticles allows one to vary the structural properties of smectic LCs [14] and to enhance the performance of devices based on both the nematic LCs [15–20] and ferroelectric LCs [21].

Recent x-ray scattering experiments on $BaTiO_3$ nanoparticle dispersions showed that they induced a one-dimensional nanostructure in nematic LC 4-*n*-pentyl-4′-cyanobiphenyl that does not exhibit a smectic phase. Thus, $BaTiO_3$ nanoparticles in soft materials can cause the formation of novel soft phases. In rare cases, doped thermotropic LCs with *n*-alkyl solvents, such as *n*-heptane [22] or *n*-dodecane [23], exhibit additional liquid crystalline phases.

In this work, nanoparticle-induced smectic phases were obtained and studied in five homologues of the 4-*n*-alkyl-4′-cyanobiphenyl homologous series. The smectic phases were not observed in doped neat compounds, but in a gel formed when clear solutions of each compound in *n*-heptane were doped with $BaTiO_3$ nanoparticles and excess *n*-heptane was evaporated. X-ray diffraction patterns of these gels consisted of up to nine orders of diffraction peaks from a one-dimensional nanostructure. The electron density distribution along the layer normal was extracted from the scattering data, thereby providing insight into the molecular arrangement inside the induced phase. Usually, this is not possible in LC materials, because x-ray scattering only results in very few peaks in the case of nematic (absent a layer structure) and smectic LCs due to purely sinusoidal density variation.

II. EXPERIMENTAL PROCEDURE

The initial dispersion of $BaTiO_3$ nanoparticles was prepared by milling cubic (nonferroelectric) $BaTiO_3$ with a small portion of oleic acid and *n*-heptane for 25 h [11]. This well-known process resulted in a dispersion of nanoparticles that possessed an average diameter of 9 nm. The concentration of the initial dispersion was carefully adjusted to 45 mg of

$BaTiO_3$ nanoparticles per gram. The LCs were obtained from Merck [4-*n*-pentyl-4′-cyanobiphenyl (5CB) and 4-*n*-octyl-4′-cyanobiphenyl (8CB)] and from Synthon Chemicals [4-*n*-butyl-4′-cyanobiphenyl (4CB), 4-*n*-hexyl-4′-cyanobiphenyl (6CB), and 4-*n*-heptyl-4′-cyanobiphenyl (7CB)]. Clear solutions of each LC were prepared by dissolving 0.1 g of the LC in 0.2 g of *n*-heptane in Eppendorf Standard micro test tubes. Subsequently, 20 mg of the turbid nanoparticle dispersion was added to each test tube. The test tubes were sealed with Parafilm to prevent evaporation of heptane. These initially turbid mixtures were stored in sealed micro test tubes at room temperature. They transformed into white gels within ≈72 h. Additional samples of doped 5CB and 8CB were prepared where the preparation method was varied in order to purify the gels and quantitatively study the yield. A solution of 0.1 g of the LC (5CB or 8CB) and 0.2 g of *n*-heptane was prepared in a centrifuge glass tube. In the next step, several samples were prepared while systematically varying the nanoparticle concentration, sealed with Parafilm, and stored for ≈72 h at room temperature. The samples were then centrifuged, leading to a separation of LC-rich white gel in the lower part of the tube and a LC-poor clear solution in *n*-heptane in the upper part. These clear solutions were decanted to glass vessels. Both the glass vessels and the centrifuge glasses were placed in a fume hood to allow *n*-heptane to evaporate until they showed mass constancy. The final weights of doped LC (upside-down triangles) and the final weights of recovered neat LC (upright triangles) are plotted versus the initial quantity of nanoparticles in Fig. 1. We cannot rule out the possibility of the polar glass surfaces of the (carefully rinsed) centrifuge vessels slightly and randomly diminishing the gelling caused by inorganic nanoparticles. However, the weight measurements (Fig. 1) show that the yield of sedimented doped LC (upside-down triangles) increased linearly with an increase in the initial concentration of nanoparticles. The weight of the LC before and after doping was carefully compared. A residual concentration of *n*-heptane (≈20%) was found to be present in the LC nanogels. Evidently, a small amount of *n*-heptane was stabilized and retained within the nanoparticle-induced phase.

For x-ray scattering experiments, the samples were filled in 1 mm quartz capillaries (Hilgenberg) and placed in a modified Instec (HCS402) hot stage with a temperature precision of ±0.1 °C. The hot stage was fitted with a pair of CoSm permanent magnets that produced a ∼2.5 kG *in situ* magnetic field. Two sets of x-ray scattering experiments were conducted; first the gels of 4CB, 5CB, 6CB, and 7CB were investigated at ambient temperature in a Rigaku Screen Machine. These experiments were conducted with copper $K\alpha$ radiation and a 75-mm-diam Mercury 3 CCD area detector positioned at a distance of ≈160 mm from the sample. The second set of measurements were performed on centrifuged doped 5CB and 8CB gel samples at the Advanced Photon Source (beamline 6-ID-B) with 0.765 335 Å synchrotron radiation and a MAR345 image plate detector placed at a distance of ≈470 mm. The diffraction data were collected at 30 and 50 °C and analyzed with FIT2D [24] and MATLAB (Rev. R2012b).

III. RESULTS

A high-intensity small-angle peak was obtained for all samples as expected from the inorganic nanoparticles. The intensity versus scattering vector q plots were generated by azimuthal integration of the two-dimensional patterns. The first set of results on gel samples is shown in Fig. 2 for the q range of 0.5–6 nm^{-1} peaks corresponding to the d spacing 4.57 and 4.51 nm, respectively. A Bragg reflection at q = 1.376 nm^{-1} (4CB, 6CB) or at 1.394 nm^{-1} (5CB, 7CB) was observed along with two higher-order reflections.

The 4CB-gel sample had a waxlike appearance while other gel samples were much softer. However, the diffraction pattern of the 7CB-gel sample differed from those of 4CB, 5CB, and 6CB samples. The latter three samples showed diffraction patterns similar to that from a powder sample. In contrast,

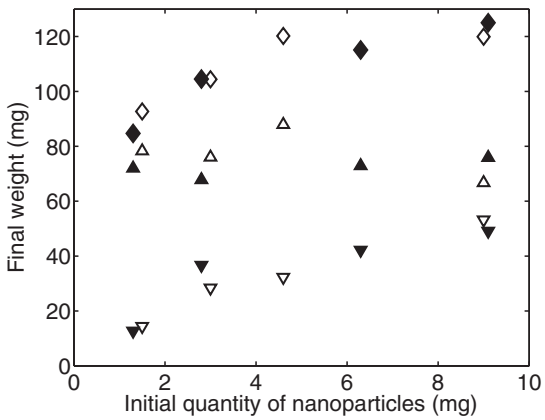

FIG. 1. The final weight of doped LC, for both 5CB (open symbols) and 8CB (filled symbols), is shown against the initial quantity of nanoparticles. Centrifugation of nanoparticle/*n*-heptane/LC gels and subsequent evaporation of *n*-heptane yielded (sedimented) doped LC (upside-down triangles) and a recovery of neat LC (triangles).

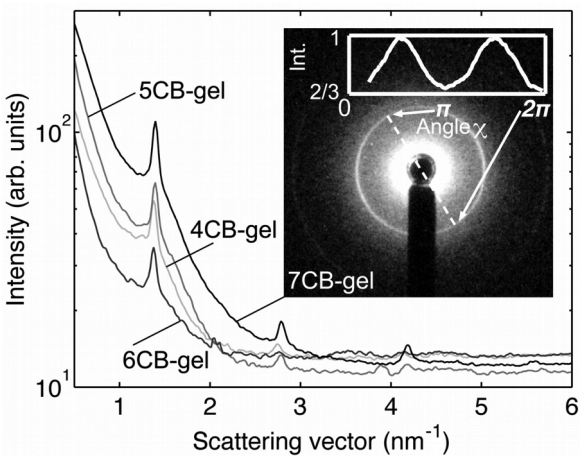

FIG. 2. Scattering profiles of gel samples of 4CB, 5CB, 6CB, and 7CB LCs. The inset shows the central region of the 2D scattering pattern in the 7CB-gel sample. The scattering pattern of 7CB is oriented: An intensity vs azimuthal angle scan is shown to quantify the orientation of the scattering pattern. The dashed secant is a guide to the eye and indicates the orientation of the scattering pattern; the orientation of the molecular long axis is perpendicular to it.

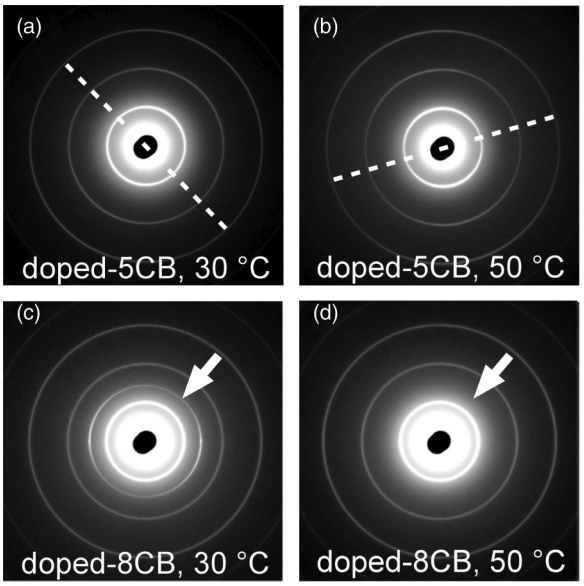

FIG. 3. Central regions of the two-dimensional diffraction patterns of (a) doped 5CB at 30 °C, (b) doped 5CB at 50 °C, (c) doped 8CB at 30 °C, and (d) doped 8CB at 50 °C. Dashed lines, drawn as a guide to the eye, indicate the orientation of the diffraction patterns and are perpendicular to the preferred orientation of the molecular long axis. The white arrows indicate the position of the SmA_d peak seen at 30 °C in (c) but absent at 50 °C in (d).

the three diffraction rings of the 7CB gel indicated a preferred orientation (indicated by an intensity versus azimuthal angle χ scan of the first diffraction ring in the inset in Fig. 2) of the molecules.

Doped 5CB and 8CB samples were further investigated with synchrotron x-ray diffraction. Figures 3(a) and 3(b) represent diffraction patterns from oriented doped-5CB samples. The orientation (indicated by a dashed line) is pronounced and thus easily seen in the diffraction pattern recorded at 50 °C [Fig. 3(b)]. Intensity versus azimuthal angle χ scans of the first-order diffraction rings are shown in Fig. 4 as dashed lines. Intensity modulation of the first diffraction ring

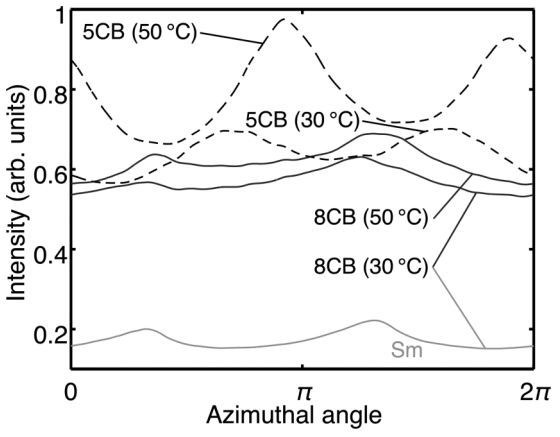

FIG. 4. Azimuthal angle χ scans of the first-order diffraction rings at different temperatures in doped 5CB (black dashed lines) and doped 8CB (solid black lines). Additionally, the χ scan (solid gray line) of the SmA_d peak observed for doped 8CB at 30 °C is shown.

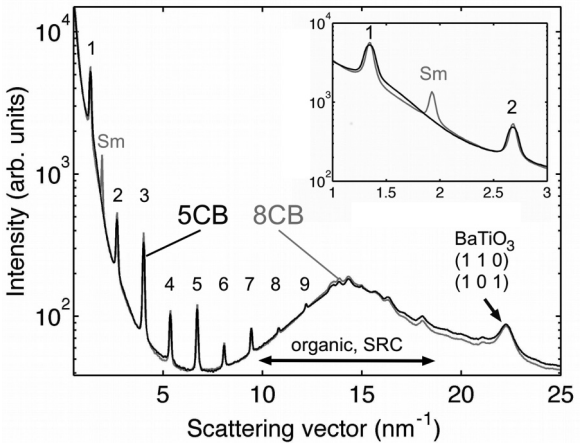

FIG. 5. Intensity vs scattering vector plots for doped 5CB (black line) almost overlap with that of the doped 8CB (gray line) at 30 °C. Nine orders of the primary diffraction peak corresponding to 4.65 nm are indicated by numbers 1 to 9. The scattering arising from transverse short-range correlations among LC molecules is indicated by the horizontal double arrow. The composite peak corresponding to the (1 1 0) and (1 0 1) reflections of $BaTiO_3$ nanoparticles is indicated by the arrow. The inset shows x-ray scattering in the small-angle region on a magnified scale.

is more pronounced for doped 5CB at 50 °C than at 30 °C. Two reflections were seen in a diffraction pattern of doped 8CB at a temperature of 30 °C. Figure 3(c) shows a multiring pattern with an additional scattering signal indicated by the arrow which is characteristic of the partial bilayer smectic A_d phase (SmA_d) [25] of neat 8CB. Although the orientation of this SmA_d signal was not as pronounced as usually observed in neat 8CB, its orientation is approximately parallel to the magnetic field as in the neat 8CB. This SmA_d signal was not present in the diffraction pattern recorded at higher temperature 50 °C [Fig. 3(d)]. The χ scans of the first ring of the two multiring patterns and of the SmA_d signal at 30 °C are shown (Fig. 4). The χ scan of the SmA_d ring at 30 °C (marked as "Sm") consists of two peaks. The maxima of both χ scans shown for a temperature of 30 °C in Fig. 4 appear at the same azimuthal angles. Accordingly, one cannot rule out the possibility of the coexistence of a nanoparticle-induced multilayer phase and the SmA_d phase of the neat LC.

The scattering curves (Fig. 5) were extracted by azimuthal integration of the diffraction patterns shown in Fig. 4 over a q range of 0.5–25 nm^{-1}. In the wide-angle range, a broad peak is present at approximately $q = 22$ nm^{-1}. To account for this peak, diffraction patterns of $BaTiO_3$ were simulated with POWDERCELL (Version 2.4). Cubic $BaTiO_3$ possesses a perovskite-type crystal lattice (space group $Pm\text{-}3m$) with a lattice constant of 0.4058 nm (JCPDS No. 75-0215 [26]), while tetragonal $BaTiO_3$ (space group $P4mm$) has $a = 0.3992$ nm and $c = 0.4036$ nm [27,28]. The calculated diffraction pattern yields the most intense (1 1 0) peak ($d = 0.2869$ nm) at $q = 21.9$ nm^{-1}. The (1 0 1) and (1 1 0) reflections are not degenerate in tetragonal $BaTiO_3$, where the (1 0 1) reflection ($d = 0.2838$ nm, $q = 22.14$ nm^{-1}) and the (1 1 0) reflection ($d = 0.2823$ nm, $q = 22.26$ nm^{-1}) had the highest and second highest peak intensities, respectively.

TABLE I. Position (q), amplitude (A), full width at half-maximum (FWHM), and normalized scattering intensities (I_{norm}) obtained from Lorentzian fits to the nine multiples of the $d \approx 4.65$ nm peak for both 8CB and 5CB at 30 and 50 °C.

Diff. Order	0th	1st	2nd	3rd	4th	5th	6th	7th	8th
8CB, 30 °C:									
q (nm^{-1})	1.345	2.681	4.021	5.365	6.717	8.074	9.438	10.813	12.190
A (arb. units)	520.00	37.76	36.78	7.77	10.06	2.63	3.63	0.75	1.44
FWHM (nm^{-1})	0.077	0.068	0.072	0.073	0.076	0.077	0.078	0.067	0.091
I_{norm}	1.000	0.289	0.632	0.238	0.482	0.182	0.344	0.094	0.227
8CB, 50 °C:									
q (nm^{-1})	1.345	2.681	4.021	5.363	6.715	8.072	9.433	10.804	12.185
A (arb. units)	701.300	49.205	45.151	9.639	11.683	3.136	4.266	1.211	1.504
FWHM (nm^{-1})	0.133	0.118	0.119	0.117	0.114	0.118	0.112	0.128	0.104
I_{norm}	1.000	0.376	0.776	0.295	0.560	0.217	0.404	0.150	0.237
5CB, 30 °C:									
q (nm^{-1})	1.347	2.681	4.020	5.364	6.716	8.070	9.436	10.806	12.140
A (arb. units)	591.60	55.98	47.30	9.17	11.82	3.16	4.30	0.91	1.51
FWHM (nm^{-1})	0.098	0.107	0.102	0.094	0.095	0.097	0.092	0.086	0.090
I_{norm}	1.000	0.375	0.712	0.246	0.497	0.192	0.357	0.099	0.207
5CB, 50 °C:									
q (nm^{-1})	1.344	2.675	4.012	5.354	6.703	8.055	9.417	10.783	12.164
A (arb. units)	253.671	21.296	19.328	3.941	4.866	1.310	1.829	0.406	0.770
FWHM (nm^{-1})	0.111	0.109	0.109	0.104	0.103	0.105	0.100	0.096	0.107
I_{norm}	1.000	0.332	0.679	0.246	0.477	0.185	0.354	0.103	0.249

In contrast to the simulated powder diffraction patterns, no sharp wide-angle scattering peaks were expected, because a system of $BaTiO_3$ nanoparticles was studied. Specifically, both the cubic and the stressed tetragonal nanoparticles were present in these samples, and the (1 1 0) and (1 0 1) reflections are broadened due to the finite-size effect. This leads to the composite broad peak observed at $q \sim 22$ nm^{-1}.

Due to short-range lateral positional order correlations (SRC), a broad scattering peak centered at ≈14–15 nm^{-1} is usually observed in soft phases of the calamitic mesogens 5CB and 8CB. Such a liquidlike peak is also observed in Fig. 5 (indicated by a horizontal double arrow). The corresponding $d \approx 4.3$ Å is characteristic for the average transverse intermolecular separation $d_\perp$ in cyanobiphenyls. Surprisingly, nine orders of a Bragg reflection with $d \approx 4.65$ (±0.025) nm were observed and are marked from 1 to 9 in Fig. 5. Their width for doped 5CB is much larger than that in doped 8CB (inset). The smectic peak at ≈1.9 nm^{-1} is seen in scattering curves of doped 8CB at 30 °C. The calculated $d \approx 3.3$ (±0.025) nm corresponds to smectic layer spacing of the stable SmA_d phase of the neat 8CB [14,29] at 30 °C.

The nine harmonics of the $d \approx 4.65$ nm peaks were fitted to the Lorentzian line shape to estimate the scattering amplitudes. Initially, each of the peaks was fitted individually. One Lorentzian function and a straight line as background were fitted to the second- to ninth-order peaks. For the first- and second-order peaks, a second Lorentzian centered at $q < 0.3$ nm^{-1} was added to model the intense small-angle scattering caused by the inorganic nanoparticles. The results are summarized in Table I. For 5CB at 30 °C, the full width at half-maximum (FWHM) of the Lorentzian fit to the first-order peak was fixed at 0.1 nm^{-1} and a second peak function was added. From its comparison with doped 8CB, where a small amount of smectic-like material was present in the sample, we infer that a small amount of nematic-like component was present in 5CB which contributed to the scattering near $q \approx 1.4$ nm^{-1} at 30 °C (see also the inset in Fig. 5). The scattering amplitudes thus obtained were multiplied by q^2 (Lorentz correction) in the second step of the data analysis. The Lorentz-corrected and normalized scattering intensities are listed in Table I. Additionally, a schematic of the Bragg scattering observed at the small angles is shown (Fig. 6) for both doped 5CB and 8CB at 30 °C.

The nine harmonics of the Bragg reflection arose from a multilayer structure of $d = 4.65$ nm. Similar multilayer structures with far fewer diffraction orders have been observed and analyzed in LC side chain polymers [30]. The scattering

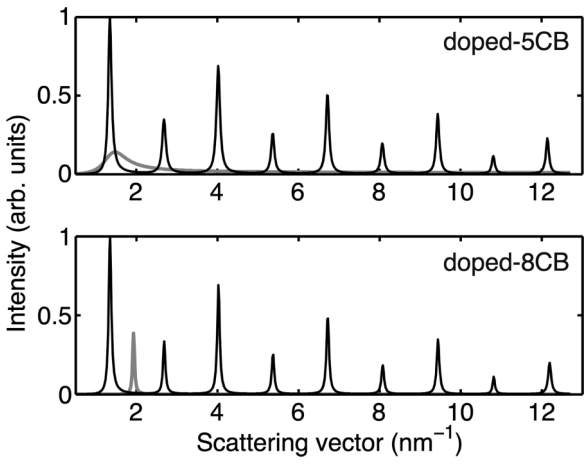

FIG. 6. Schematic scattering intensities of nine multiples of the $d \approx 4.65$ nm Bragg peak observed in doped 5CB and doped 8CB (black lines) and the residual LC (gray lines) present in doped 5CB (neat nematic phase) and doped 8CB (neat SmA_d phase) at 30 °C.

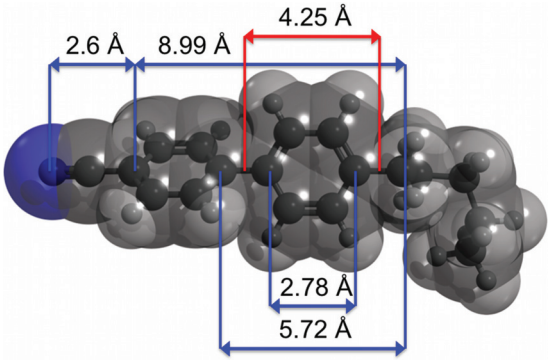

FIG. 7. (Color online) Model of 5CB and characteristic length scales of the cyanobiphenyl group and the 4′-benzylic methylene group of the alkyl chain.

amplitudes $[A_{\text{scat}}(q)]$ of such structures can be expressed as a Fourier transform of the electron density profile $\rho(z)$ in the z direction perpendicular to the layers:

$$A_{\text{scat}}(q) = \int_{-d/2}^{d/2} \rho(z) e^{-iqz} dz. \quad (1)$$

The electron density profile can be extracted from the n measured scattering amplitudes from the inverse Fourier transform in terms of cosine functions when a symmetric electron density profile is expected:

$$\rho(z) = \sum_n A_n \cos\left(\frac{n2\pi z}{d}\right). \quad (2)$$

The modulus of the scattering amplitudes $|I_{\text{norm}}^{0.5}|$ can be directly calculated since the intensities were recorded. However, their signs remain indeterminate (the phase problem). A common method to obtain the sign is to calculate the 2^n electron density profiles described by Eq. (2) and compare them to what sign one should expect from a possible molecular arrangement [30]. Accordingly, the 5CB molecule was visualized using the open-source software Avogadro [31,32] in order to estimate the size of the characteristic molecular building blocks (Fig. 7). The molecular model clearly shows that the terminal cyanophenyl moiety is twisted with respect to the central phenyl moiety of the molecule. Each of these resonance-stabilized building blocks possesses a relatively high and delocalized electron density which is higher than the average electron density in the alkyl chain.

After careful examination of the calculated electron density profiles, the phase combination [+ - - + - - + + -] was selected. To show the accuracy of this phase combination, molecular models of 5CB and 8CB were scaled and their relative electron density versus layer spacing (Fig. 8) plotted. It should be noted that Fig. 8 represents the average relative electron density distributions inside the soft phases and not the electron density of a single molecule. Nevertheless, superposition of the molecular model over the electron density profile is instructive and shows that the cyanobiphenyl group leaves a footprint on the shown relative electron density profiles. The two peaks observed in the electron density profiles fit the characteristic spacing of the electron-rich moieties of the cyanobiphenyl group. A drop in the electron density is observed at the position of the alkyl chain. The layer spacing

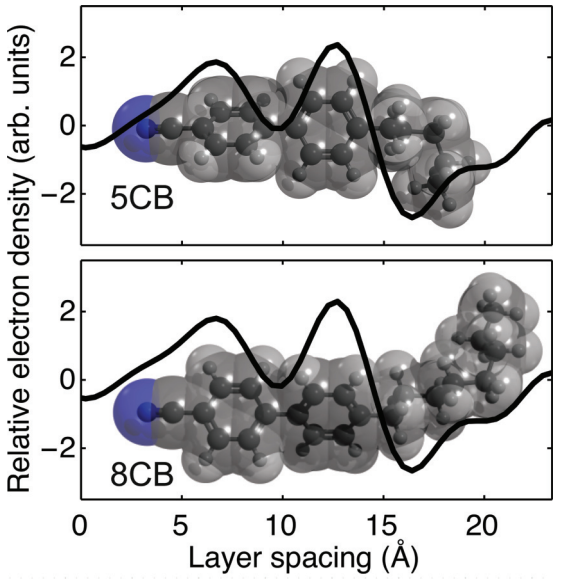

FIG. 8. (Color online) Molecular model of 5CB and 8CB superimposed on plots of the relative electron density vs layer spacing. Only one-half of the symmetric bilayer is shown.

is equal to twice the molecular length in both phases. Thus, the molecular arrangement in the present phase is comparable to the bilayer SmA_2 phase [25]. However, in contrast to the present nanoparticle-induced phase, such a large number of higher orders of the small-angle peak are never observed in neat thermotropic systems. The molecular arrangement in thermotropic phases of n-alkyl-cyanobiphenyls can be very well understood in atomistic simulations under the assumption that the alkyl tails favor an all-*trans* conformation [33]. A schematic of the molecular arrangement is shown (Fig. 9) for the 5CB and n-heptane molecules. The molecules are

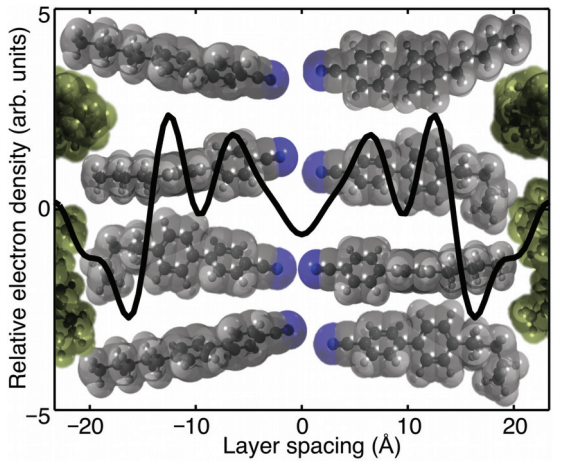

FIG. 9. (Color online) Plot of the relative electron density in the direction perpendicular to the smectic layers. Since the relative electron density distribution corresponds to the average distribution in the coherent scattering volume, more than two molecules have to be considered to describe the molecular arrangement in smectic layers. Molecular models of eight 5CB molecules and two n-heptane molecules are schematically shown to illustrate molecular arrangement in the smectic bilayer.

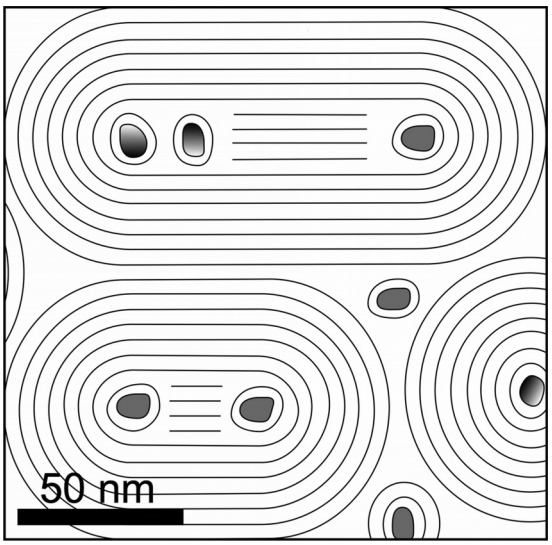

FIG. 10. Two-dimensional schematic of the structure inside a small volume of a nanoparticle-doped sample. Three polar nanoparticles (gradient filled) and five nonpolar nanoparticles (uniformly filled) are shown. A surface layer of 4-*n*-alkyl-4′-cyanobiphenyl molecules is grafted to the surface of the inorganic nanoparticles. The black lines indicate the interfaces of the soft bilayers that form multishells.

found to possess a short-range positional order within the bilayers, and the alkyl chains are allowed to move freely in the nanoparticle-induced phase.

Upon heating the samples from 30 to 50 °C, the FWHM of the fitted Lorentzian peaks of doped 5CB increased only slightly from ≈0.10 to ≈0.11 nm^{-1}. The correlation length (2π/FWHM) of the multilayers was ≈60 nm, or 12–13 layers at the higher temperature. Heating the doped 8CB sample led to an increase of the FWHM from ≈0.07 to ≈0.12 nm^{-1}. Accordingly, the correlation length in doped 8CB decreased from 90 to 52 nm (from 19 to 11 layers).

The relative electron density profiles along the z direction are presented for both doped 5CB and doped 8CB in Fig. 9. Near the center, these profiles show a variation of the relative electron density that is characteristic for a head-to-head arrangement of cyanobiphenyl groups. The variation of electron density is much smaller in the aliphatic region and plays a relatively insignificant role in x-ray diffraction from multilayer structures. Nevertheless, one can speculate that the aliphatic chains of the 4-*n*-alkyl-4′-cyanobiphenyl molecules are stabilized by London interactions. The multilayer phase shows a general layer spacing of 4.5 nm for all studied homologues, and ≈20% of *n*-heptane are stabilized in the nanostructure. The remainder of *n*-heptane appears to be stabilized in the aliphatic part of the 4-*n*-alkyl-4′-cyanobiphenyl bilayers. Using the concentration of approximately 15% of nanoparticles in the systems investigated, a density of $BaTiO_3$ of 6 g/cm^3, and 1 g/cm^3 for the density of the organic materials, we estimate that the nanoparticles will comprise about 2.5% of the sample volume. Therefore, eight nanoparticles may be present in a 9-nm-thick layer with a size of ≈160 nm × 160 nm. Based on this assumption, a two-dimensional schematic of a thin layer of a nanoparticle-doped sample is shown (Fig. 10). Both polar nanoparticles (gradient filled) and nonpolar nanoparticles (uniformly filled) are shown. A monolayer of 5CB is grafted onto the surface of these inorganic nanoparticles. The nanoparticles are surrounded by multilayer shells of *n*-heptane-stabilized 4-*n*-alkyl-4′-cyanobiphenyl bilayers. The aliphatic bilayer interfaces are indicated by black lines. Due to the irregular shape of nanoparticles, these shells are most likely elliptical rather than perfectly spherical. A phase that consists of nonoriented, elliptically shaped multishells would lead to powder (nonoriented) x-ray diffraction patterns. In addition, samples may also appear to be weakly oriented because the ellipses may become oriented in the magnetic field. Alternatively, pairing or formation of strings (or chains) of polar nanoparticles may also lead to cigar-shaped multishells more prone to orient in an external field. Oriented scattering patterns were observed in 7CB gel (with an unknown heptane content), doped 5CB, and doped 8CB. The orientation effects in 5CB and 8CB were more pronounced at higher temperature. One can speculate whether the higher chain length of 7CB and 8CB leads to more stable cigar-shaped multishells and thus to a more pronounced orientation observed in the scattering patterns. Presumably, repeated heating and cooling in a magnetic field could also generate the higher degree of orientation as observed at higher temperatures.

IV. CONCLUSIONS

In conclusion, evidence presented here clearly shows the impact of nanoparticle doping on the phase behavior and molecular organization of small mesogenic polar molecules in which the rigid part of the molecule, and not the overall molecular length, determines the layer spacing of the induced self-assembled nanostructure. These investigations of one-dimensional soft nanostructures are very useful as they reveal detailed information about the molecular arrangement in the multilayers. The results also provide evidence for a preferred orientation of soft modified phases in an external field. The technique employed in this study is suitable to test other mesogens and presumably even nonmesogens in order to study the nature of molecular associations induced by the presence of nanoparticle in soft phases. This method has great potential to produce alignment layers for use in LC devices, to achieve memory effects, and as a method to induce and investigate novel phases in other self-assembling photonic structures, such as chiral nematic and chiral smectic LCs.

ACKNOWLEDGMENTS

Research was supported by the German Research Foundation (Grants No. KI 411/14, No. GRK 1464, and No. LO 1922/1-1). Participation of S.K. and DMA in this project was supported by the U.S. Department of Energy (DOE), the Office of Science (OS), Basic Energy Sciences (BES) Grant No. DE-SC0001412. Use of the Advanced Photon Source, an Office of Science User Facility operated for the Argonne National Laboratory, was supported by the U.S. DOE, BES under Contract No. DE-AC02-06CH11357. The molecular models were created with Avogadro [31] and rendered by using POV-Ray [33].

[1] H. Qui and T. Hegmann, J. Mater. Chem. **18**, 3288 (2008).
[2] O. Stamatoiu, J. Mirazaei, X. Feng, and T. Hegmann, in *Liquid Crystals: Materials Design and Self-assembly*, edited by C. Tschierske, Topics in Current Chemistry, Vol. 318 (Springer, Berlin, Heidelberg, 2012), p. 331.
[3] G. L. Nealon, R. Greget, C. Dominguez, Z. T. Nagy, D. Guillon, J.-L. Gallani, and B. Donnio, Beilstein J. Org. Chem. **8**, 349 (2012).
[4] M. Wojcik, W. Lewandowski, J. Matraszek, J. Mieczkowski, J. Borysiuk, D. Pociecha, and E. Gorecka, Angew. Chem., Int. Ed. **48**, 5167 (2009).
[5] A. V. Glushchenko, G. Y. Guba, N. Y. Lopukhovich, V. M. Ogenko, V. Y. Reshetnyak, Y. A. Reznikov, and O. V. Yaroshchuk, Mol. Cryst. Liq. Cryst. **262**, 111 (1995).
[6] M. Urbanski, B. Kinkead, T. Hegmann, and H.-S. Kitzerow, Liq. Cryst. **37**, 1151 (2010).
[7] R. Eidenschink and W. H. De Jeu, Electron. Lett. **27**, 1195 (1991).
[8] M. Kreuzer, T. Schudi, W. H. de Jeu, and R. Eidenschink, Appl. Phys. Lett. **62**, 1712 (1993).
[9] S. Relaix, R. L. Leheny, L. Reven, and M. Sutton, Phys. Rev. E **84**, 061705 (2011).
[10] Y. Shi, B. Cull, and S. Kumar, Phys. Rev. Lett. **71**, 2773 (1993).
[11] H. Atkuri, G. Cook, D. R. Evans, C.-I. Cheon, A. Glushchenko, V. Reshetnyak, Y. Reznikov, J. West, and K. Zhang, J. Opt. A **11**, 024006 (2009).
[12] S. A. Basun, G. Cook, V. Y. Reshetnyak, A. V. Glushchenko, and D. R. Evans, Phys. Rev. B **84**, 024105 (2011).
[13] G. Cook, J. L. Barnes, S. A. Basunm, D. R. Evans, R. F. Ziolo, A. Ponce, V. Y. Reshetnyak, A. Glushchenko, and P. P. Banerjee, J. Appl. Phys. **108**, 064309 (2010).
[14] A. Lorenz, N. Zimmermann, S. Kumar, D. R. Evans, G. Cook, M. Fernández Martínez, and H.-S. Kitzerow, J. Phys. Chem. B **117**, 937 (2013).
[15] O. Buchnev, A. Dyadyusha, M. Kaczmarek, V. Reshetnyak, and Y. Reznikov, J. Opt. Soc. Am. B **24**, 1512 (2007).
[16] G. Cook, A. Glushchenko, V. Reshetnyak, A. T. Griffith, M. A. Saleh, and D. R. Evans, Opt. Express **16**, 4015 (2008).
[17] A. Glushchenko, C. I. Cheon, J. West, F. Lic, E. Büyüktanir, V. Reznikov, and A. Buchnev, Mol. Cryst. Liq. Cryst. **453**, 227 (2006).
[18] F. Li, O. Buchnev, C. I. Cheon, A. Glushchenko, V. Reshetnyak, Y. Reznikov, T. J. Sluckin, and J. L. West, Phys. Rev. Lett. **97**, 147801 (2006); **99**, 219901(E) (2007).
[19] G. Cook, V. Yu. Reshetnyak, R. F. Ziolo, S. A. Basun, P. P. Banerjee, and D. R. Evans, Opt. Express **18**, 17339 (2010).
[20] A. Lorenz, N. Zimmermann, S. Kumar, D. R. Evans, G. Cook, M. Fernández Martínez, and H.-S. Kitzerow, Appl. Opt. **52**, E1 (2013).
[21] A. Rudzki, D. R. Evans, G. Cook, and W. Haase, Appl. Opt. **52**, E6 (2013).
[22] Y. Yamaoka, Y. Taniguchi, S. Yasuzuka, Y. Yamamura, and K. Saito, J. Chem. Phys. **135**, 044705 (2011).
[23] D. Krüerke, P. Rudquist, S. T. Lagerwall, H. Sawade, and G. Heppke, Ferroelectrics **243**, 207 (2000).
[24] A. P. Hammersley, ESRF Internal Report, ESRF97HA02T (1997).
[25] S. Kumar, *Liquid Crystals: Experimental Study of Physical Properties and Phase Transitions* (Cambridge University Press, Cambridge, UK, 2001).
[26] R. L. Brutchey and D. E. Morse, Angew. Chem., Int. Ed. **45**, 6564 (2006).
[27] M. M. Vijatovic, J. D. Bodic, and B. D. Stojanovic, Sci. Sintering **40**, 235 (2008).
[28] F. Jona and G. Shirane, *Ferroelectric Crystals* (Dover, New York, 1993).
[29] M. G. Lafouresse, M. B. Sied, H. Allouchi, D. O. Lopez, J. Salud, and J. L. Tamarit, Chem. Phys. Lett. **376**, 188 (2003).
[30] P. Davidson, A. M. Levelut, M. F. Achard, and F. Hardouin, Liq. Cryst. **4**, 561 (1989).
[31] Avogadro Ver 1.1.0., M. D. Hanwell, D. E. Curtis, D. C. Lonie, T. Vandermeersch, E. Zurek, and G. R. Hutchison, J. Cheminformatics **4**, 17 (2012).
[32] Persistence of Vision Pty. Ltd. (2004). Persistence of Vision (TM) Raytracer. Persistence of Vision Pty. Ltd., Williamstown, Victoria, Australia.
[33] N. F. Palermo, A. Pizzirusso, L. Muccioli, and C. Zannoni, J. Chem. Phys. **138**, 204901 (2013).